Title: Sacrificial Crystal Templating of Hyaluronic Acid-Based Hydrogels.

Authors: Richelle C. Thomas [a,b,c], Paul E. Chung [b], Shan P. Modi [a], John G. Hardy [a,c,]*, Christine E. Schmidt [a,c,]*

Affiliations:

[a] Department of Biomedical Engineering, The University of Texas at Austin, Austin, TX, USA

[b] McKetta Department of Chemical Engineering, The University of Texas at Austin, Austin, TX, USA

[c] J. Crayton Pruitt Department of Biomedical Engineering, The University of Florida, Gainesville, FL, USA

Emails: thomas.richelle@gmail.com (R.C.T.); paul.chung@utexas.edu (P.C.); shanmodi13@gmail.com (S.P.M.); johnhardyuk@gmail.com (J.G.H.), schmidt@bme.ufl.edu (C.E.S.).

*Authors to whom correspondence should be addressed:

J. Crayon Pruitt Department of Biomedical Engineering, The University of Florida, Gainesville, FL 32601; E-mail: johnhardyuk@gmail.com (J.G.H.), schmidt@bme.ufl.edu (C.E.S.); Tel:+1-352-273-9222; Fax: +1-352-273-9221.

ABSTRACT:

Natural tissues have intricate structures organized in a hierarchical fashion over multiple length scales (Å to cm). These tissues commonly incorporate pores as a key feature that may regulate cell behavior. To enable the development of tissues scaffolds with biomimetic pore structures, it is important to investigate methods to impart pores to biomaterials, such as the use of novel sacrificial porogens. Here we report the use of sacrificial crystals to impart pores to biopolymer hydrogels (based on a methacrylated hyaluronic acid derivative) with macroscopic crystal templated pores embedded within them. The pore structure was investigated using microscopy (cryoSEM and confocal), and the specific sacrificial porogen used was found not only to impact the pore structure, but also swelling and mechanical properties. Such templated hydrogels have prospects for application as instructive tissue scaffolds (where the pore structure controls cell alignment, migration etc.).

Keywords: hydrogel; sacrificial porogen; pore structure; tissue scaffold; biomaterials

Main text:

1. Introduction

Hydrogels are a useful *in vitro* platform for studying how structure-property relationships impact cell-material interactions, and may offer insight into the behavior of natural tissues *in vivo*. The development of hydrogels with biomimetic chemical compositions is popular; however, it is noteworthy that it is possible to impart a range of porosities to the hydrogels, enabling mimicry of natural pore structures found *in vivo*. The range of pore structures facilitate three-dimensional cell cultures *in vitro* that are more representative of *in vivo* conditions and may therefore reduce/replace our reliance on animal models for biological studies, an area of strategic importance for the sustainable development of affordable healthcare technologies in the future by governmental funding bodies including the National Institute of Health in the United States, and the Research Councils in the UK [1-3]. This opportunity motivated us to develop a simple and reproducible methodology for generating novel pore structures inside hydrogels that may be of use for investigations pertaining to the effect that architecture has on the biological/mechanical properties of tissue scaffolds.

Hydrogels with isotropic pores have been extensively investigated for application as tissue scaffolds. In recent years, there has been growing interest in the development of hydrogels with more complex pore structures. Hydrogels with micropores and macropores have been created by solvent casting/particle leaching [4], freeze drying [5], layer-by-layer composition [6], and rapid prototyping [7]; each methodology having strengths and weaknesses. Sacrificial porogen leaching is popular, and may, in certain cases allow the pore size/shape to be controlled by appropriate choice of the porogen [4, 8-12]. Freeze-drying ice-crystal templated hydrogels is an environmentally friendly method that enables the generation of aligned pores in hydrogels [13, 14], and rapid prototyping enables the generation of complex 3D structures [15-21].

Here we report the results of our investigation of the use of sacrificial crystals as templates for hyaluronic acid-based hydrogels. Solutions of a photocrosslinkable hyaluronic acid derivative and porogens that undergo thermally-induced crystallization drive phase separation to polymer-rich and poor phases. Photocrosslinking the hyaluronic acid derivative yields a continuous polymer network around the organized crystal porogens that may be selectively removed, leaving a characteristic pore structure within the hydrogel. Indeed, we have previously reported that the properties of hydrogels [22] can be markedly altered using such sacrificial porogens in 2D hydrogels [23], and here we extend this to generate 3D hydrogels.

Four sacrificial crystal templates were studied (glycine, guanidine, urea and potassium dihydrogen phosphate), the removal of which was observed to create a specific porous network within the hydrogel. The architectures generated may be useful for biomimetic tissue scaffolds [24] for vascular [8], bone [25], cartilage [27], and neural [28] tissue niches, particularly because we employ hyaluronic acid (a natural component of the extracellular matrix) as the polymer matrix of the hydrogels [29].

2. Experimental

2.1. Materials

High molecular weight sodium hyaluronate from *Streptococcus equi* of molecular weight 1.6×10^6 Da (Sigma 53747), glycidyl methacrylate (Sigma 779342), triethylamine (Sigma T0886), hyaluronidase (Sigma H3506) and dextran-FITC of molecular weight 3,000-5,000 Da (Sigma FD4) were all purchased from Sigma Aldrich. Urea (Fisher U15), potassium dihydrogen phosphate (Fisher 7778), glycine (Fisher G48) and guanidine hydrochloride (Fisher BP178), phosphate-buffered saline (PBS, Sigma P4417) were obtained from Sigma Aldrich or Fisher, as determined by their availability. The photoinitiator Irgacure 2959 (55047962) was obtained from Ciba Specialty Chemicals/BASF. The PhosphoWorks™ Fluorimetric Phosphate Assay Kit *Red Fluorescence (21660) was purchased from AAT Bioquest. The Urea Fluorometric Assay Kit (700620) was purchased from Cayman Chemical. Fluval Clearmax (A1348) phosphate remover was purchased from PetCo, Inc. All reagents were used as received.

2.2. Hydrogel Preparation

Hydrogels at 20 mg/mL methacrylated hyaluronic acid (methacrylation of the primary alcohol was observed for ca. 18% of the disaccharides in hyaluronic acid) [29] with 0.3% (w/v) photoinitiator were templated with each of the porogens. The porogens were mixed into the warm (~50 °C) polymer solutions. The supersaturated polymer solution was injected into disk molds (Grace Biolabs Silicone Isolators #664301) encased by two glass slides and cooled on ice to cause porogen precipitation within the polymer solution. After crystallization, the polymer was crosslinked around the crystalline network by exposing the hydrogel to 13 mW/cm^2 ultra-violet light, and the crystals were removed by immersing the hydrogel in deionized water overnight to remove the crystalline component, then swollen in 10 mM phosphate-buffered saline for 24h.

2.3. Cryopreservation Scanning Electron Microscopy

Cryogenic scanning electron microscopy (CryoSEM) was used to examine the microstructure of the samples that were fixed to the mounting stage with carbon tape and carbon paint. The samples were then flash frozen in liquid nitrogen (at −195 °C), sublimated, sputter coated with platinum, and imaged using a Zeiss Supra 40VP SEM [29-31].

2.4. Confocal Laser Scanning Microscopy

Confocal microscopy was used to study the dimensions of the pores of samples that were incubated in a 1 mg/mL dextran-FITC (Sigma) solution in water overnight and subsequently rinsed in deionized water for 24-48h to reduce any background signal. Confocal images were taken on Leica SP2 AOBS Microscope in z-stack mode. The acquired images were compiled using IMARIS software or ImageJ with the Volume Viewer 2.0 plug-in to create three-dimensional renderings of the pores.

2.5. Swelling Studies

A swelling study was conducted using the gravimetric method [32-36]. The swelling ratio was evaluated using the porogen-free hydrogels that were swollen in 10 mM PBS overnight, after which excess PBS was carefully blotted away and the swollen weight was recorded, then oven-dried

overnight to obtain the dry weight of the polymer. To determine equilibrium water content (EWC), the crystal-free hydrogels were allowed to reach equilibrium in deionized water and the weight recorded. The samples were then dried overnight in an oven to achieve the weight of the polymer component in the hydrogel samples (data presented is from a minimum of 8 samples as the mean ± standard error of the mean).

2.6. Flory-Huggins calculations

The swell ratio was calculated using equation (1):

(1) Swell ratio = $(W_s-W_d)/W_d$

where W_s is the swollen weight of the sample, and W_d is the weight of the dried sample [35-36]. The equilibrium water content (the EWC), i.e. percentage of water within the hydrogel, was calculated using equation (2):

(2) EWC (%, w/w) = $((W_e-W_d)/W_e)*100$

where W_e is the swollen weight of the sample at equilibrium, and W_d was obtained after oven drying the hydrogels until a constant weight was reached [32-36]. The degree of swelling can be estimated using Flory-Huggins swelling theory [29]. The ratio of the swollen mass in pure water to the dried mass is the degree of mass swelling Q_M, calculated using equation (3):

(3) $Q_M = M_{Swollen}/M_{Dry}$

The degree of mass swelling relates to the volumetric swelling ratio, Q_v, through the densities of the polymer and solvent, calculated using equation (4) [29]:

(4) $Q_V = 1 + \rho_p/\rho_s(Q_M-1)$

The dry polymer density, ρ_p, for hyaluronic acid is 1.229 g/cm^3 [29] and the density of the solvent (water) is 1 g/cm^3. The volumetric swelling ratio is related to the molecular weight between crosslinks via the molar volume of the solvent, the Flory interaction parameter of the polymer, and the solvent. According to Leach et al, the interaction parameter (χ) for HA-water is 0.473 [29, 37]. The molar volume of water, V_1, is 18.1 cm^3/mol. Therefore the molecular weight between crosslinks ($\overline{M_C}$), can be calculated using equation (5):

(5) $Q_V^{5/3} \approx \frac{\overline{\upsilon M_C}}{V_1}(\frac{1}{2} - X)$

The swollen hydrogel mesh size (ξ) is related to the root initial square radius $\overline{r_o^2}$, calculated using equation (6) [38]:

(6) $\xi = Q_V^{1/3}\sqrt{\overline{r_o^2}}$

Cleland et al found that $\frac{\overline{r_o^2}}{2n} = 2.4nm$ [39] which allows simplification of equation 6 to equation (7)

$\xi = 0.1748\sqrt{\overline{M_c}} \, Q_V^{1/3}$

Equation 7 relates the $\overline{M_C}$ to the mesh size and allows the estimation of mesh size without knowing the unperturbed distance. The effective crosslink density, υ_e, is the ratio of the polymer density to the molecular weight between crosslinks, calculated using equation (8) [29, 39]:

$$(8) \; \upsilon_e = \frac{\rho_p}{\overline{M_C}}$$

In swollen, crosslinked structures the equilibrium polymer volume fraction, υ_e, is inversely proportional to equilibrium volume degree of swelling, Q_v [38, 39].

2.7. Mass Change Experiments

Mass change experiments were conducted to understand the porogen release kinetics. Freshly prepared hydrogels (immediately after photocrosslinking) were individually immersed in 3 mL of deionized water to remove the porogen and weighed at interval time points until equilibrium was reached. For both the urea and potassium dihydrogen phosphate-templated hydrogels, the procedure included with the assay kits were followed (the PhosphoWorks™ Fluorimetric Phosphate Assay Kit was supplied by AAT Bioquest, and the Urea Fluorometric Assay Kit was supplied by Cayman Chemical). For the urea fluorometric assay kit, the ammonia detector was warmed at 37 °C to help its dissolution in ethanol. For urea-templated hydrogels, the dilutions of the eluted solution required to be detected by the assay kit for each day were as follows: Day 1 – 1:103, Day 2 – 1:102, Day 3 – 1:102, Day 4 – 1:102. Days 5-7 were not diluted. For potassium dihydrogen phosphate-templated hydrogels, the re-quired dilutions were as follows: Day 1 – 1:3.5x103, Day 2 – 1:3.5x102, Day 3 – 1:35 (6μL in 210μL). Days 4-7 were not diluted. For the potassium dihydrogen phosphate-templated hydrogels, phosphate free water was created by dialyzing the phosphate remover against approximately 4L of water for a minimum of 7 days. This water was used for the phosphate ion detection. For the potassium dihydrogen phosphate-templated gels, the incubation time used was 1 hour, and the background wells contained 60μL Assay Buffer and 40μL of the sample. A Synergy HT microplate reader was used to analyze the samples. The porogen release data was normalized to the hydrogel weight at 270 minutes after water immersion. Hydrogel mass data were plotted on a log-log scale in order to determine the characteristic exponent n and characteristic constant k of the Koresmeyer-Peppas equation [33, 34]. Because the model best suits linear data, the linear portion of the plot was isolated to gain the swell-release kinetic values. The linear portion from log-log plots of the data suits the model and ranged from 8-25 minutes (data is presented from a minimum of 6 samples as the mean ± standard error of the mean). To quantify the transport mechanism of solute and water into the hydrogel system, swelling data was fit to the Korsmeyer-Peppas equation [33, 34] that is typically employed to describe solute diffusion in polymers, calculated using equation (9):

$$(9) \; M_t/M_\infty = kt^n$$

M_t is the mass of water absorbed or mass of molecule released at time t, M_∞ is the mass of water absorbed at equilibrium, k is a characteristic constant of the hydrogel and n is the characteristic exponent of the mode of transport of the penetrating media.

2.8. Rheology

Rheology experiments were conducted on PBS-swollen hydrogels using 25 mm parallel plates. An amplitude sweep with the storage modulus as a function of strain was performed to identify the

linear region of the viscoelastic curve. Measurements were conducted at constant strain over a frequency sweep of 0.1-10 Hz. GMHA hydrogels (20 mg/ml) with I2959 (0.3% w/v, mg/ml) exposed to 5 minutes UV were analyzed at 25°C on an Anton Paar rheometer with approximately 2 mm gap size (data is presented from a minimum of 6 samples as the mean ± standard error of the mean). A strain sweep was conducted for each type of hydrogels to determine the most appropriate value for the frequency sweep. Strain values were selected at approximately the mid-point of the linear region of the strain sweep. The strain for each hydrogel type is as follows: not templated hydrogels (0.05% strain), potassium dihydrogen phosphate-templated hydrogels (0.05%), urea-templated hydrogels (0.05% strain) and glycine-templated hydrogels (5% strain).

2.9. Degradation

For degradation experiments, a solution of 50 U/mL hyaluronidase in 10 mM PBS was used to degrade the photocrosslinked hydrogels. The PBS swollen hydrogels were placed in 1 mL of hyaluronidase solution and incubated at 37°C. The initial hydrogel weight was recorded and recorded every hour for 12 hours thereafter (or until complete hydrogel dissolution), and data is presented from a minimum of 6 samples as the mean ± standard error of the mean. The *in vitro* degradation profile of the hydrogels was evaluated by recording the hydrogel weights after swelling in saline (W_o) and at specific times during hyaluronidase enzymatic degradation (W_t), calculated using equation (10) [37]:

(10) % Degradation = $((W_o-W_t)/W_o)*100$

2.10. Cell Viability Experiments

Hydrogels were suspended in cell culture medium in transwell plates (Corning) to verify the viability of cells in the presence of the scaffolds. The experiment determined cell viability in the presence of any potential leachable from the hydrogels; cells were not in direct contact with the hydrogels. Schwann cells and fibroblasts were cultured for 48 hours with hydrogels suspended in media and Cell Titer Glo (Invitrogen) assay used to determine their viability. Two luminescence readings were taken from each sample and the quantitative values averaged.

3. Results and discussion

3.1. Hydrogel Architecture

We report a simple method of imparting macropores to hyaluronic acid-based hydrogels using sacrificial crystal templates. We used a methacrylated hyaluronic acid derivative (Fig. 1), prepared in accordance with the literature [29], where methacrylation of the primary alcohol was observed for ca. 18% of the disaccharides in hyaluronic acid. It is noteworthy that the templating methodology would be applicable to a broad range of water soluble polymers (e.g. polyethylene glycols, proteins) [22, 23, 40, 41, 42, 43]. The void regions within the hydrogel samples were imaged by cryoSEM (Fig. 2) and confocal microscopy (Fig. 3). The cryoSEM images for each sample show the crystal templating methodology to be effective [44-47]. Hydrogels that were not templated (Fig. 2A) had surfaces that lacked defined void regions in line with other images for analogously prepared hydrogels. The surface of glycine crystal templated hydrogels (Fig. 2B) showed small pores imparted by the glycine of up to ca. 2 μm in width and ca. 10 μm in length; the surface of guanidine crystal templated hydrogels (Fig. 2C) showed much finer pores with lengths/widths of less than 1 μm; the

surface of potassium dihydrogen phosphate crystal templated hydrogels (Fig. 2D) have pores with lengths/widths of greater than 10 μm, as did the urea crystal templated hydrogels (Fig. 2E). Confocal microscopy images for the not templated hydrogels and glycine-templated hydrogels were very diffuse and without any easily discernible macroscopic voids. By contrast, confocal microscopy (Fig. 3) revealed void spaces imparted to the hydrogels by guanidine crystal templated hydrogels showed the presence of cuboid voids of 10-100 μm (Fig. 3A), elongated voids of 10s to 100s of μm in width and length, respectively (Fig. 3B), imparted by the potassium dihydrogen phosphate crystals; and the urea crystals imparted elongated voids spaces of 10s to 100s of μm in width and lengths of over 1000 μm in the hydrogels (Fig. 3C), with some evidence of urea crystal alignment (in line with our previous reports) [22, 23, 40, 41, 42, 43]. The macropore structures resemble the negative imprint of the sacrificial crystals inside the hydrogel matrix, and crystal templated hydrogels possess a larger void volume than comparable hydrogels without the sacrificial porogen, and the pores imparted to the hydrogels using our methodology should be cell-permeable by virtue of their size.

3.2. Hydrogel physical and mechanical properties

The physical properties of the hydrogels were studied to elucidate the effect of each porogen (Table 1). The porogens were used at concentrations that were the minimum at which we were able to thermally induce crystallization of the porogen, which was roughly associated with the solubility of the porogen at 25 °C in water. The protocol was optimized for rapid crystal formation as the hydrogel solution cooled and relatively low concentrations of crystals to obtain gels which could be easily handled. The EWC is defined as the amount of water within a hydrogel after it has equilibrated in water, and while the EWCs of the hydrogels was similar (96% to 99%, (w/w), there was more variation in the swell ratios for the hydrogels which was 38-57 for the macroporous hydrogels, and 69 for the control hydrogels without macropores, suggesting that the control hydrogels without the sacrificial porogens were less tightly crosslinked. Based on these experimental values it is possible to calculate the degree of mass swelling (Q_M), the equilibrium volume degree of swelling (Q_v), the average molecular weight of polymer chains between neighbouring crosslinks ($\overline{M_C}$), the mesh size (ξ) and the effective network density (υ_e). The not templated hydrogels had a mesh size of ca. 2572 nm, whereas the templated gels had mesh sizes of 548 to 1859 nm, suggesting that the sacrificial porogens force the polymer chains to pack more tightly prior to photocrosslinking. While the data suggests that glycine, guanidine and urea interact with the polymer chains similarly, these interactions are weaker than those for potassium dihydrogen phosphate. This tighter packing leads to a corresponding reduction in the effective mesh size of the gels, and explains the marked differences in swell ratios of the macroporous gels and not templated control hydrogels. The swell ratio for hydrogels templated with urea was a function of both the extent of crosslinking [49, 50] and the weight percent of photoinitiator. The swelling ratio increased with urea templating at both 0.5% (w/v) and 1% (w/v) photoinitiator concentrations (Fig. 4), and as the porogen concentration increased, so did the swell ratio (Fig. 5), offering another simple method to tune the hydrogel properties to more accurately mimic a specific tissue niche [48, 49].

The porogen leaching process was studied by observing changes in hydrogel mass over time to provide insight into the process of porogen release and hydrogel swelling (Fig. 6) upon water immersion to remove the porogen [24]. Guanidine crystal templated samples initially lost mass before recovering to a mass that was less than the original weight; potassium dihydrogen phosphate-templated hydrogels initially gained mass before retracting to approximately their

original mass; glycine and urea crystal templated hydrogels increased to three and four times their original mass upon immersion in water, respectively. The samples then reached their maximum plateau mass. Table 1 and Figure S1 show the n and k values obtained for all samples suggesting that sacrificial porogen release kinetics were non-Fickian, which was expected because Fickian diffusion relies upon the hydrogel being completely amorphous [50].

The bulk mechanical properties of hydrogel scaffolds play a role in their performance *in vivo*, and the gels must be mechanically robust enough to withstand mechanical loading and stresses that occur in the specific niche in which they are used in the body. Rheological experiments were performed under oscillatory shear stress to determine the effect of templating on the hydrogel's mechanical properties (in this case storage modulus, G' [40]). We observed that the elastic modulus was affected by crystal templating (Fig. 7). Not templated gels had the highest storage modulus, G' ca. 100 Pa. suggests that a decrease in the storage modulus by about an order of magnitude occurred for crystal templated samples. This confirms that micrometer scale pores in the hydrogels have an impact on the mechanical properties of the hydrogels, and offers a method to tune the mechanics of the hydrogels to suit a specific biological niche.

3.3. Degradation, porogen leaching and gel cytotoxicity

Hydrogels may degrade by hydrolysis, enzymatic degradation or dissolution [51-54]. Biopolymers are widely used for hydrogels in tissue engineering because of their ability to be degraded *in vivo* by naturally occurring enzymes, indeed, hyaluronic acid is degraded by the naturally occurring enzyme hyaluronidase [53, 54]. The *in vitro* degradation profile is an indicator of the effective crosslink density as more tightly crosslinked hydrogels tend to degrade more slowly. Improved enzyme penetration throughout the hydrogel's volume as a result of templating is thought to enhance the rate of degradation. Indeed, templated samples degraded significantly more quickly than not templated hydrogels of the same chemical composition (Fig. 8). The degradation rate *in vivo* would be controlled by the concentration of hyaluronidase in the specific tissue in which the biomaterial is implanted, and our *in vitro* data supports the fact the hydrogels are susceptible to enzymatic degradation (i.e. not too highly crosslinked for the enzyme to cleave the backbone of the hyaluronic acid).

Ideally tissue engineering constructs should display little or no cytotoxicity, consequently the phosphate ion and urea concentrations in effluent media from templated hydrogels at specific points in time (displayed in Table S1 and Fig. S2). After three days of rinsing, the concentration of phosphate ions was less than the systemic phosphate levels in adult human blood, whereas the urea templated samples release urea at concentration that is below the systemic urea levels in blood after four days of rinsing. Furthermore the cytotoxicity of the rinsed hydrogels were evaluated on fibroblasts and Schwann cells and compared with a negative control of 10% (v/v) dimethylformamide in cell culture media. The error bars for cell viability of fibroblasts and Schwann cells (Fig. 9) cultured in the presence of urea-templated hydrogels overlap with those from the positive control culture plate or experimental control with not templated hydrogels suggest that the templated hydrogels have a negligible effect on cell viability.

4. Conclusion

The development of biomimetic tissue scaffolds is a promising avenue of research for tissue engineering, and pore structure is an important feature of natural tissues. A simple, bench-top process using inexpensive sacrificial crystal templates was adapted [22, 23] to create complex architecture within three-dimensional photopolymerized hydrogels, and yields hydrogels that can be easily handled in the lab with pore structures resembling some natural tissues, representing a useful platform for *in vitro* studies of pore architecture on cellular behaviour [55]. We also speculate that the sacrificial crystal templates could serve a secondary role as a therapeutic agent [56] delivered over a sustained period of time, yielding a tissue scaffold that instructs cell behavior not only because of its architecture, but also the action of the bioactive drug [56].

Acknowledgement

Appendix A. Supplementary material

Supplementary data associated with this article can be found, in the online version, at:

References

[1] J. Patterson, M. M. Martino, J. A. Hubbell, Biomimetic materials in tissue engineering. Materials Today 13(2010) 14-22.

[2] M. Schindler, A. Nur-E-Kamal, I. Ahmed, J. Kamal, H.-Y. Liu, N. Amor, A. S. Ponery, D. P. Crockett, T. H. Grafe, H. Y. Chung. Living in three dimensions. Cell Biochemistry and Biophysics 45(2006) 215-227.

[3] H. R. Irons, D. K. Cullen, N. P. Shapiro, N. A. Lambert, R. H. Lee, M. C. LaPlaca. Three-dimensional neural constructs: a novel platform for neurophysiological investigation. J. Neural Engineering 5 (2008) 333.

[4] C. Martinez-Ramos, A. Valles-Lluch, J. M. Verdugo, J. L. Ribelles, J. A. Barcia Albacar, A. B. Orts, J. M. Soria Lopez, M. M. Pradas. Channeled scaffolds implanted in adult rat brain. J. Biomed. Mater. Res. A. 100 (2012) 3276-86.

[5] P. Z. Elias, M. Spector. Treatment of penetrating brain injury in a rat model using collagen scaffolds incorporating soluble Nogo receptor. J. Tissue Eng. Regen. Med. 9 (2012) 137-150.

[6] T. Zhang, Y. Yan, X. Wang, Z. Xiong, F. Lin, R. Wu, R. Zhang. Three-dimensional gelatin and gelatin/hyaluronan hydrogel structures for traumatic brain injury. Journal of Bioactive and Compatible Polymers 22 (2007) 19-29.

[7] T. Billiet, M. Vandenhaute, J. Schelfhout, S. Van Vlierberghe, P. Dubruel. A review of trends and limitations in hydrogel-rapid prototyping for tissue engineering. Biomaterials 33 (2012) 6020-6041.

[8] M. C. Ford, J. P. Bertram, S. R. Hynes, M. Michaud, Q. Li, M. Young, S. S. Segal, J. A. Madri, E. B. Lavik. A macroporous hydrogel for the coculture of neural progenitor and endothelial cells to form functional vascular networks in vivo. Proc. Natl. Acad. Sci. USA 103 (2006) 2512-7.

[9] C. J. Liao, C. F. Chen, J. H. Chen, S. F. Chiang, Y. J. Lin, K. Y. Chang. Fabrication of porous biodegradable polymer scaffolds using a solvent merging/particulate leaching method. J. Biomedical Materials Research 59 (2002) 676-681.

[10] Y. S. Nam, J. J. Yoon, T. G. Park. A novel fabrication method of macroporous biodegradable polymer scaffolds using gas foaming salt as a porogen additive. J. Biomedical Materials Research 53 (2000) 1-7.

[11] Y. S. Nam, T. G. Park. Biodegradable polymeric microcellular foams by modified thermally induced phase separation method. Biomaterials 20 (1999) 1783-1790.

[12] Y. S. Nam, T. G. Park. Porous biodegradable polymeric scaffolds prepared by thermally induced phase separation. J. Biomedical Materials Research 47 (1999) 8-17.

[13] G. Chen, T. Ushida, T. Tateishi. Scaffold design for tissue engineering. Macromolecular Bioscience 2 (2002) 67-77.

[14] C. Ji, A. Khademhosseini, F. Dehghani. Enhancing cell penetration and proliferation in chitosan hydrogels for tissue engineering applications. Biomaterials 32 (2011) 9719-9729.

[15] B. V. Slaughter, S. S. Khurshid, O. Z. Fisher, A. Khademhosseini, N. A. Peppas. Hydrogels in regenerative medicine. Advanced Materials 21 (2009) 3307-3329.

[16] J. A. Burdick, G. D. Prestwich. Hyaluronic acid hydrogels for biomedical applications. Advanced Materials 23 (2011) H41-H56.

[17] J. G. Torres-Rendon, T. Femmer, L. De Laporte, T. Tigges, K. Rahimi, F. Gremse, S. Zafarnia, W. Lederle, S. Ifuku, M. Wessling, J. G Hardy, A. Walther. Bioactive gyroid scaffolds formed by sacrificial templating of nanocellulose and nanochitin hydrogels as instructive platforms for biomimetic tissue engineering. Advanced Materials 27 (2015) 2989-2995.

[18] Y. Luo, M. S. Shoichet. A photolabile hydrogel for guided three-dimensional cell growth and migration. Nat. Mater. 3 (2004) 249-253.

[19] J. A. Burdick, K. S. Anseth. Photoencapsulation of osteoblasts in injectable RGD-modified PEG hydrogels for bone tissue engineering. Biomaterials 23 (2002) 4315-4323.

[20] A. Sannino, M. Madaghiele. Tuning the porosity of collagen-based scaffolds for use as nerve regenerative templates. Journal of Cellular Plastics 45 (2009) 137-155.

[21] W. L. Murphy, R. G. Dennis, J. L. Kileny, D. J. Mooney. Salt fusion: an approach to improve pore interconnectivity within tissue engineering scaffolds. Tissue Engineering 8 (2002) 43-52.

[22] S. A. Zawko, C. E. Schmidt. Crystal templating dendritic pore networks and fibrillar microstructure into hydrogels. Acta Biomater. 6 (2010) 2415-21.

[23] S. Zawko, C. E. Schmidt. Giving hydrogels backbone: Incorporating physical architecture into soft biomaterials. SurFACTS in Biomaterials 17 (2012) 13-14.

[24] C. E. Schmidt, J. B. Leach. Neural tissue engineering: strategies for repair and regeneration. Annual Review of Biomedical Engineering 5 (2003) 293-347.

[25] D. W. Hutmacher. Scaffolds in tissue engineering bone and cartilage. Biomaterials 21 (2000) 2529-2543.

[27] K. M. Park, Y. K. Joung, K. D. Park, S. Y. Lee, M. C. Lee. RGD-conjugated chitosan-pluronic hydrogels as a cell supported scaffold for articular cartilage regeneration. Macromolecular Research 16 (2008) 517-523.

[28] N. Gomez, Y. Lu, S. Chen, C. E. Schmidt. Immobilized nerve growth factor and microtopography have distinct effects on polarization versus axon elongation in hippocampal cells in culture. Biomaterials 28 (2007) 271-284.

[29] J. Baier Leach, K. A. Bivens, C. W. Patrick Jr, C. E. Schmidt, Photocrosslinked hyaluronic acid hydrogels: natural, biodegradable tissue engineering scaffold. Biotechnology and Bioengineering 82 (2003), 578-589.

[30] J. P. van Duynhoven, I. Broekmann, A. Sein, G. M. van Kempen, G. J. W. Goudappel, W. S. Veeman. Microstructural investigation of monoglyceride–water coagel systems by NMR and CryoSEM. Journal of colloid and interface science 285 (2005) 703-710.

[31] A. K. Jha, M. S. Malik, M. C. Farach-Carson, R. L. Duncan, X. Jia. Hierarchically structured, hyaluronic acid-based hydrogel matrices via the covalent integration of microgels into macroscopic networks. Soft Matter 6 (2010) 5045-5055.

[32] X. Z. Zhang, D. Q. Wu, C. C. Chu. Synthesis, characterization and controlled drug release of thermosensitive IPN–PNIPAAm hydrogels. Biomaterials 25 (2004) 3793-3805.

[33] N. Dafader, M. Adnan, M. Haque, D. Huq, F. Akhtar. Study on the properties of copolymer hydrogel obtained from acrylamide/2-hydroxyethyl methacrylate by the application of gamma radiation. African Journal of Pure and Applied Chemistry 5 (2011) 111-118.

[34] J. Ruiz, A. Mantecon, V. Cadiz. Synthesis and properties of hydrogels from poly (vinyl alcohol) and ethylenediaminetetraacetic dianhydride. Polymer 42 (2001) 6347-6354.

[35] S. W. Kim, Y. H. Bae, T. Okano. Hydrogels: Swelling, Drug Loading, and Release. Pharmaceutical Research 9 (1992) 283-290.

[36] D. R. Rohindra, A. V. Nand, J. R. Khurma. Swelling properties of chitosan hydrogels. The South Pacific Journal of Natural and Applied Sciences 22 (2004) 32-35.

[37] S. Van Vlierberghe, P. Dubruel, E. Schacht. Biopolymer-Based Hydrogels As Scaffolds for Tissue Engineering Applications: A Review. Biomacromolecules 12 (2011) 1387-1408.

[38] T. Canal, N. A. Peppas. Correlation between mesh size and equilibrium degree of swelling of polymeric networks. Journal of Biomedical Materials Research 23 (1989) 1183-1193.

[39] R. L. Cleland. Ionic polysaccharides. IV. Free-rotation dimensions for disaccharide polymers. Comparison with experiment for hyaluronic acid. Biopolymers 9 (1970) 811-824.

[40] J. G. Hardy, C. E. Ghezzi, R. J. Saballos, D. L. Kaplan, C. E. Schmidt, Supracolloidal assemblies as sacrificial templates for porous silk-based biomaterials. International Journal of Molecular Sciences 16 (2015), 20511-20522.

[41] F. M. Lee, L. E. Lahti. Solubility of urea in water-alcohol mixtures. Journal of Chemical and Engineering Data 17 (1972) 304-306.

[42] D. Erdemir, S. Chattopadhyay, L. Guo, J. Ilavsky, H. Amenitsch, C. U. Segre, A. S. Myerson. Relationship between self-association of glycine molecules in supersaturated solutions and solid state outcome. Physical Review Letters 99 (2007) 115702.

[43] P. A. Barata, M. L. Serrano. Thermodynamic representation of the solubility for potassium dihydrogen phosphate (KDP)+ water+ alcohols systems. Fluid Phase Equilibria 141 (1997) 247-263.

[44] R. A. Gemeinhart, J. Chen, H. Park, K. Park. pH-sensitivity of fast responsive superporous hydrogels. Journal of Biomaterials Science, Polymer Edition 11 (2000) 1371-1380.

[45] J. M. González-Méijome, A. López-Alemany, J. B. Almeida, M. A. Parafita, M. F. Refojo. Microscopic observations of superficial ultrastructure of unworn siloxane-hydrogel contact lenses by cryo-scanning electron microscopy. Journal of Biomedical Materials Research Part B: Applied Biomaterials 76 (2006) 419-423.

[46] Y. Qiu, K. Park. Superporous IPN hydrogels having enhanced mechanical properties. AAPS PharmSciTech 4 (2003) 406-412.

[47] J. Kim, M. J. Yaszemski, L. Lu. Three-dimensional porous biodegradable polymeric scaffolds fabricated with biodegradable hydrogel porogens. Tissue Engineering Part C: Methods 15 (2009) 583-594.

[48] C. G. Williams, A. N. Malik, T. K. Kim, P. N. Manson, J. H. Elisseeff. Variable cytocompatibility of six cell lines with photoinitiators used for polymerizing hydrogels and cell encapsulation. Biomaterials 26 (2005) 1211-1218.

[49] S. J. Bryant, C. R. Nuttelman, K. S. Anseth. Cytocompatibility of UV and visible light photoinitiating systems on cultured NIH/3T3 fibroblasts in vitro. Journal of Biomaterials Science, Polymer Edition 11 (2000) 439-457.

[50] D. De Kee, Q. Liu, J. Hinestroza. Viscoelastic (Non-Fickian) Diffusion. The Canadian Journal of Chemical Engineering, 83 (2005) 913-929.

[51] J. L. Drury, D. J. Mooney. Hydrogels for tissue engineering: scaffold design variables and applications. Biomaterials 24 (2003) 4337-4351.

[52] F. Brandl, F. Sommer, A. Goepferich. Rational design of hydrogels for tissue engineering: Impact of physical factors on cell behavior. Biomaterials 28 (2007) 134-146.

[53] E. J. Menzel, C. Farr. Hyaluronidase and its substrate hyaluronan: biochemistry, biological activities and therapeutic uses. Cancer Letters 131 (1998) 3-11.

[54] K. S. Girish, K. Kemparaju. The magic glue hyaluronan and its eraser hyaluronidase: A biological overview. Life Sciences 80 (2007) 1921-1943.

[55] N. Annabi, J. W. Nichol, X. Zhong, C. Ji, S. Koshy, A. Khademhosseini, F. Dehghani. Controlling the porosity and microarchitecture of hydrogels for tissue engineering. Tissue Engineering Part B: Reviews 16 (2010) 371-383.

[56] F. Zhao, M. L. Ma, B. Xu. Molecular hydrogels of therapeutic agents. Chemical Society Reviews 38 (2009) 883-891.

Figures and Captions:
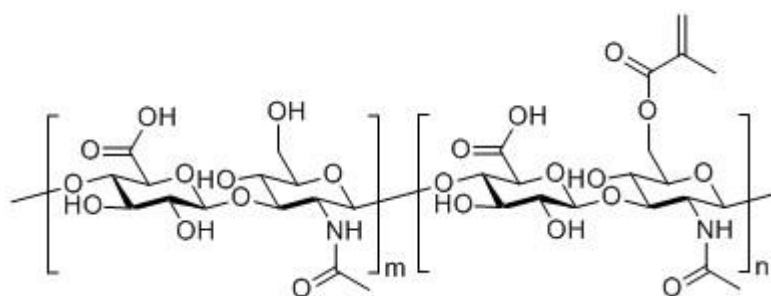
Fig. 1. Methacrylated hyaluronic acid derivative.
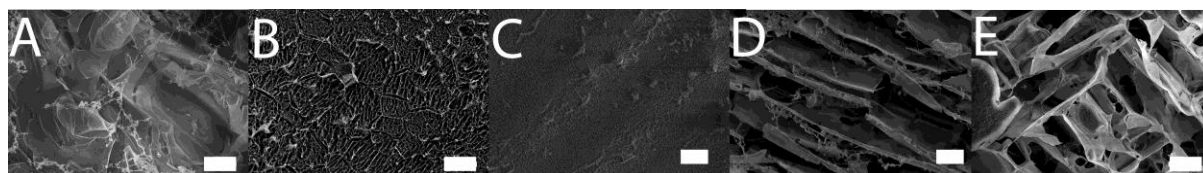
Fig. 2. Cryo-SEM images of hydrogel architecture. A) Not templated hydrogels. B) Glycine templated hydrogels. C) Guanidine templated hydrogels. D) Potassium dihydrogen phosphate templated hydrogels. E) Urea templated hydrogels. Scale bars represent 10 μm.
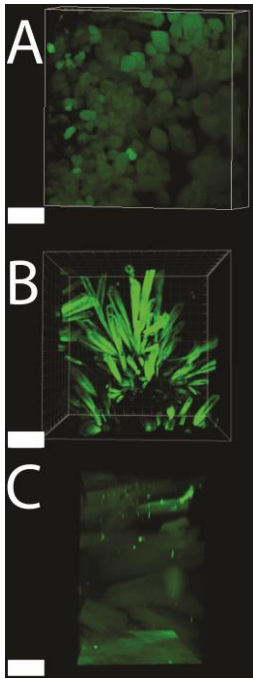
Fig. 3. Stack of confocal microscope images shows voids in crystal templated hydrogels. A) Glycine templated hydrogel, scale bar represents 200 μm. B) Potassium dihydrogen phosphate templated hydrogel, scale bar represents 300 μm. C) Urea templated hydrogels, scale bar represents 500 μm.
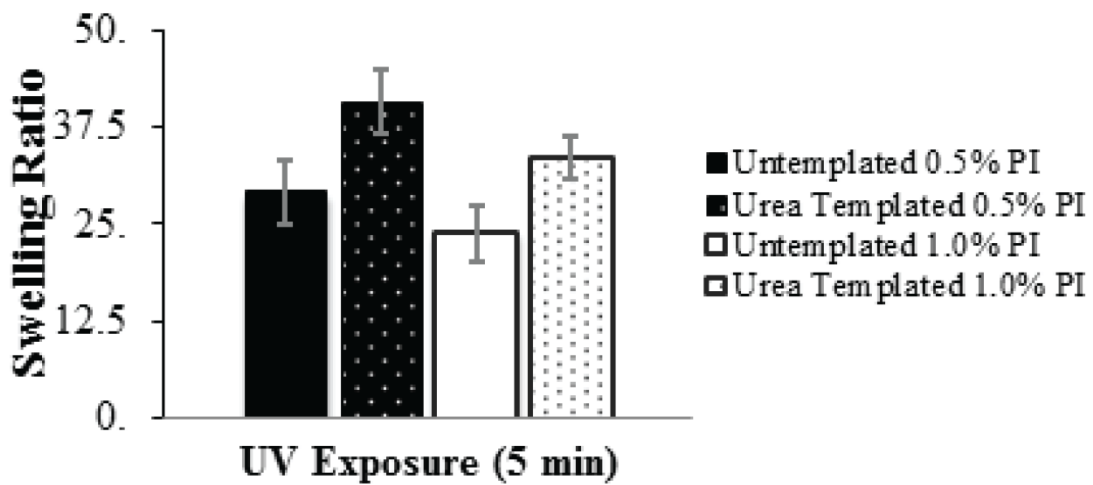
Fig. 4. The swell ratio of not templated and urea templated hydrogels was determined at two photoinitiator concentrations.
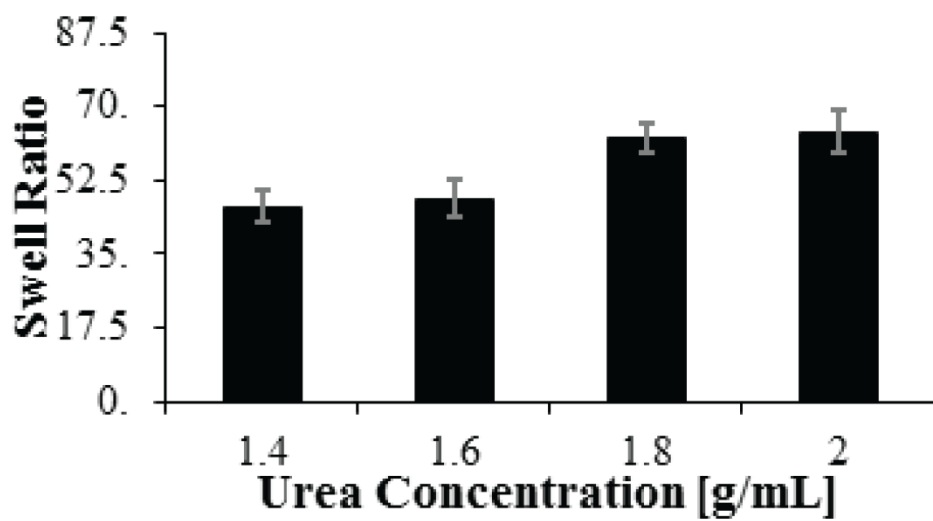
Fig. 5. Swell ratio of urea templated hydrogels with urea concentration from 1.4-2.0 g/ml.
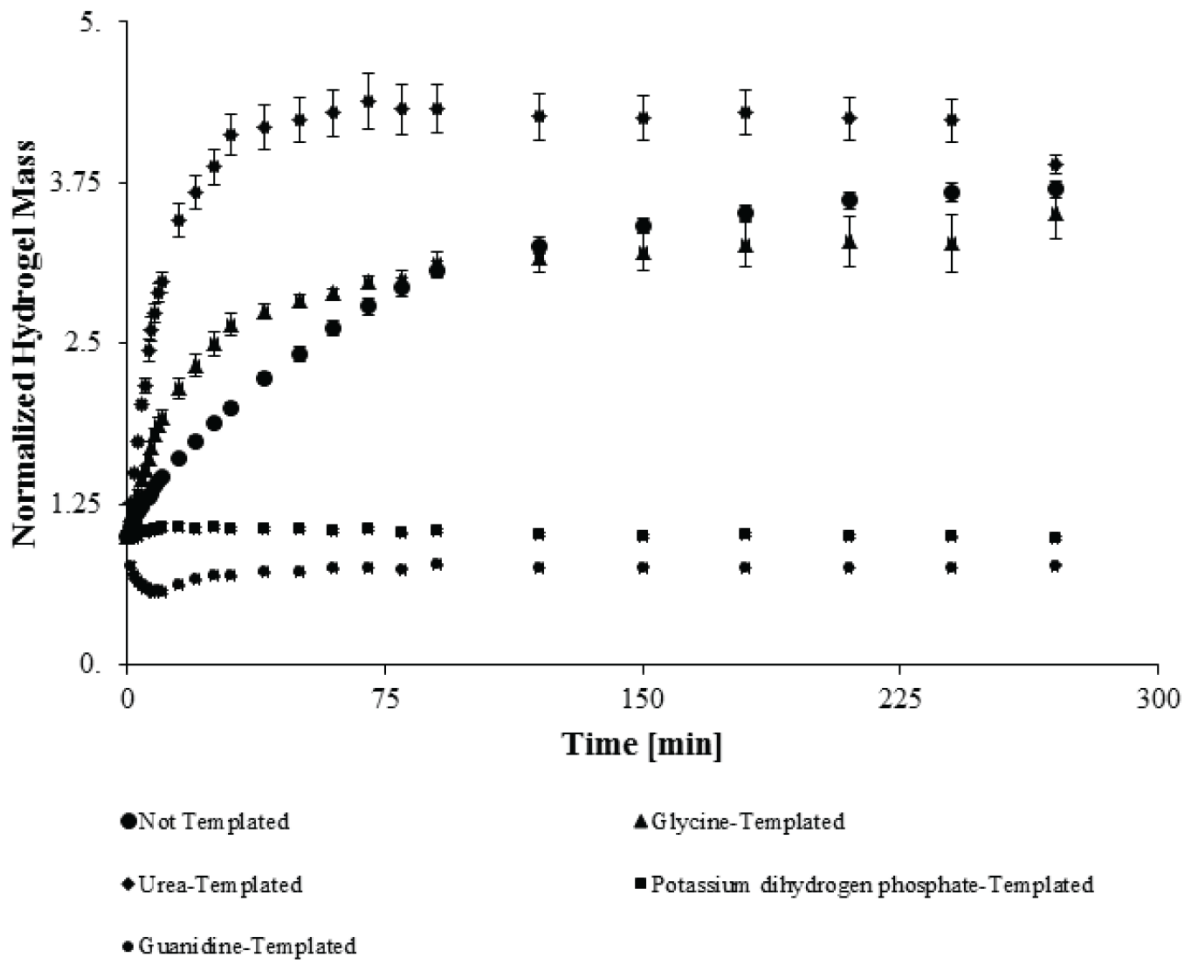
Fig. 6. Porogen leaching assay: normalized change in hydrogel mass over time.
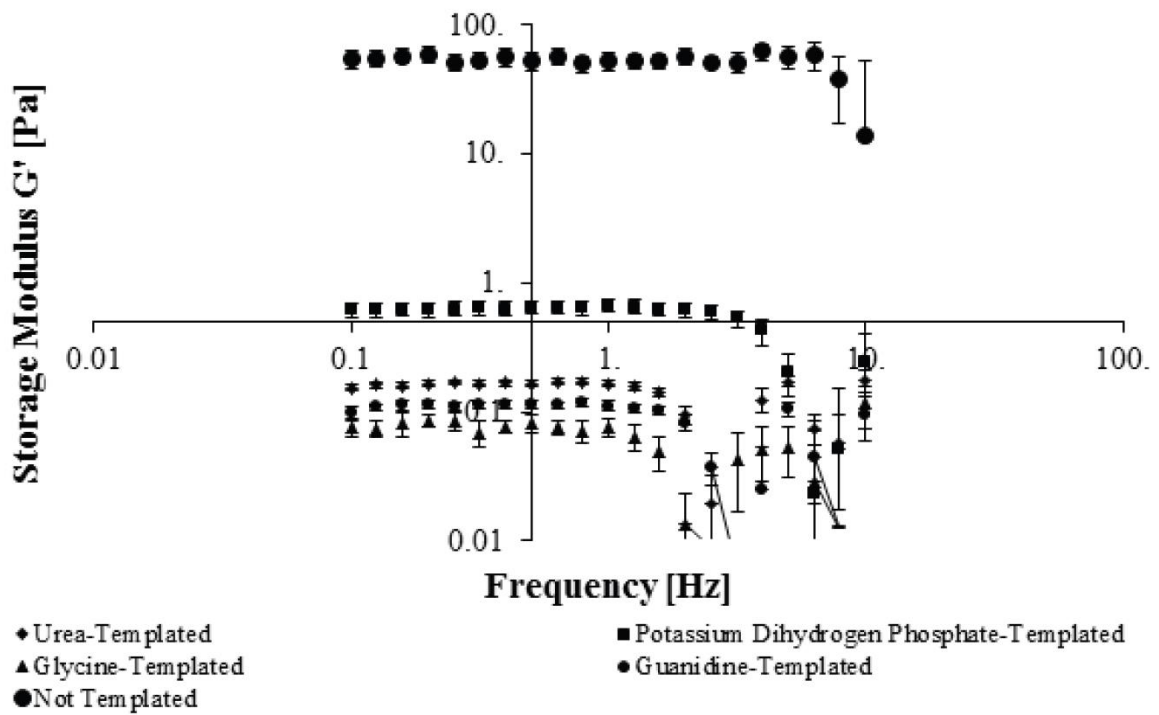
Fig. 7. Storage modulus of the hydrogels as determined by rheology.
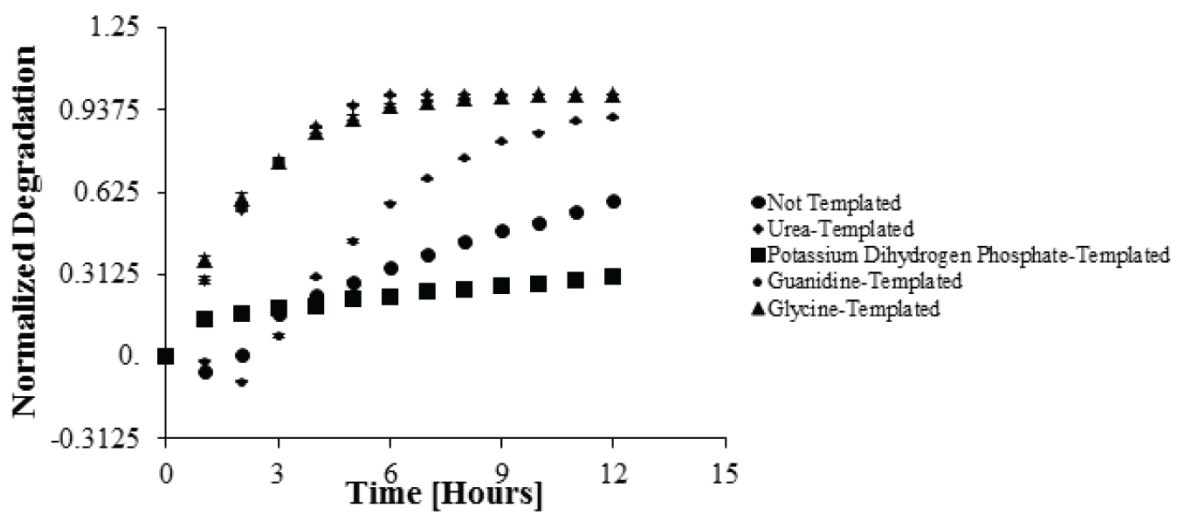
Fig. 8. Degradation behavior of the hydrogels in the presence of hyaluronidase *in vitro*.
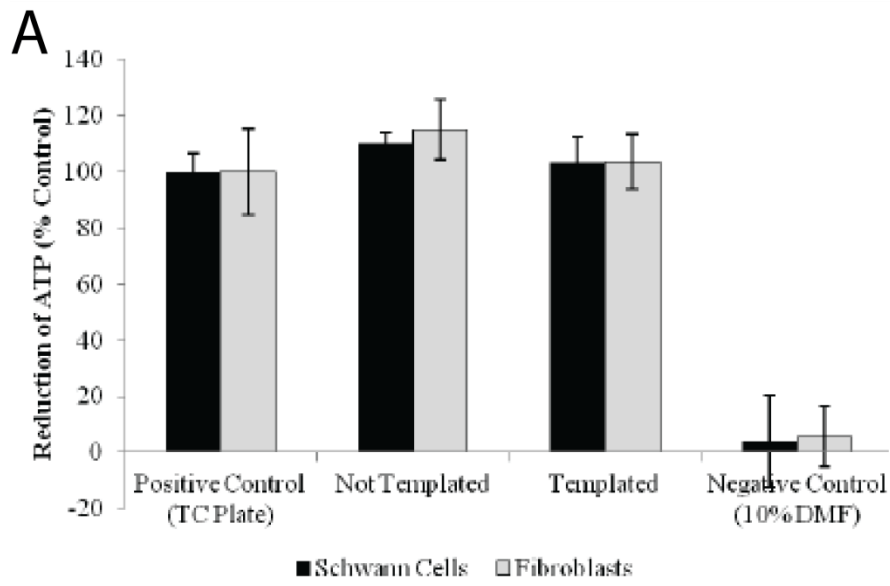
Fig. 9. Cell Titer Glo Assay of relative cell viability from 48 hours in culture of fibroblasts and Schwann cells with samples suspended in culture media. There was not a significant difference between cell viability from urea-templated and not templated hydrogels.

Tables:

Table 1. Physical characteristics values for hydrogels.

	Not templated	Glycine	Guanidine	Potassium dihydrogen phosphate	Urea
Concentration at Saturation (mg/mL)	N/A	260	2150	300	1400
Equilibrium Water Content (%, w/w)	99.6 ± 0.2	99.5 ± 0.1	96.5 ± 2.1	99.4 ± 0.4	99.6 ± 0.4
Swell Ratio	69.5 ± 2.1	53.1 ± 1.3	56.7 ± 2.8	44.0 ± 1.0	37.9 ±1.2
Q_M	140.2	106.2	82.7	37.4	79.4
Q_v	172.1	130.2	101.4	45.7	97.3
$\overline{M_C}$ (g/mol)	6997872	4400383	2899155	768892	2708156
ξ (nm)	2572	1859	1388	548	1323
υe (mol/cm^3)	1.76E-07	2.79E-07	4.24E-07	1.59E-06	4.54E-07
Time until Mass Stability (min)	90	25	8	60	9
n	0.7417	0.6967	0.2703	-0.4353	0.9091
K	0.0219	0.0689	0.7686	0.1931	0.0638

Q_M, the degree of mass swelling. Q_v, equilibrium volume degree of swelling. Average molecular weight of polymer chains between neighboring crosslinks. ξ, mesh size. υ_e, effective network density.